Steady-state solutions of hydrodynamic traffic models

H. K. Lee,[1] H.-W. Lee,[2] and D. Kim[1]

[1]*School of Physics, Seoul National University, Seoul 151-747, Korea*
[2]*Department of Physics, Pohang University of Science and Technology, Pohang, Kyungbuk 790-784, Korea*

We investigate steady-state solutions of hydrodynamic traffic models in the absence of any intrinsic inhomogeneity on roads such as on-ramps. It is shown that typical hydrodynamic models possess seven different types of inhomogeneous steady-state solutions. The seven solutions include those that have been reported previously only for microscopic models. The characteristic properties of wide jam such as moving velocity of its spatiotemporal pattern and/or out-flux from wide jam are shown to be uniquely determined and thus independent of initial conditions of dynamic evolution. Topological considerations suggest that all of the solutions should be common to a wide class of traffic models. The results are discussed in connection with the universality conjecture for traffic models. Also the prevalence of the limit-cycle solution in a recent study of a microscopic model is explained in this approach.

I. INTRODUCTION

Vehicles on roads interact with other and various traffic phenomena can be regarded as collective behaviors of interacting vehicles [1–3]. Analyses of highway traffic data revealed that there exist qualitatively different states of traffic flow [4–8]. Transition between different traffic states was also reported [5]. Some empirical findings, such as the so-called synchronized traffic flow phase [5], have become subjects of considerable concern and ignited intense theoretical investigations of traffic flow. Comprehensive reviews can be found, for example, in Ref. [9].

Many traffic flow models have been put forward and analyzed [10–21]. Quite often, the analysis aims to find out possible steady-states, or dynamic phases, of the models and investigate their properties. A criterion for good and reliable traffic models is good agreement between steady states of models and traffic states revealed via real traffic data analysis. Thus an important first step in the analysis of traffic flow models is to find out all possible steady states.

In this paper, we consider hydrodynamic models for traffic without bottlenecks such as ramps and present a systematic search for their steady-state solutions which are time-independent in a proper moving reference frame:

$$\rho(x,t) = \tilde{\rho}(x + v_g t), \quad v(x,t) = \tilde{v}(x + v_g t), \tag{1}$$

where ρ and v are density and velocity fields, respectively, and $-v_g$ is the constant velocity of the moving reference frame with respect to the stationary reference frame. Two well-known steady solutions of this type are free flow and traffic jam solutions [22–24]. Surprisingly, we find that hydrodynamic models possess not only these two but also *several* other steady-state solutions. Some of the newly recognized steady-state solutions, including limit-cycle solutions, have been reported previously only for microscopic traffic models [16,18,25] and not been reported for hydrodynamic models, which led to the widespread view that free flow and traffic jam are the only possible steady-state solutions of hydrodynamic models in the absence of bottlenecks such as

ramps. Our result shows that such view is incorrect and that the physics contained in hydrodynamic models may be much richer than previously recognized.

In Sec. II, we first review the mapping to the single-particle motion and introduce the concept of the flow diagram in the single-particle phase space. It is demonstrated in Sec. III that the flow diagram can have various topologically different structures, which are directly linked to the existence of certain types of steady-state solutions (Sec. IV). Section V discusses implications of our results. Section VI concludes the paper.

II. MAPPING TO SINGLE-PARTICLE MOTION

We consider a hydrodynamic model that consists of the following two equations, an equation for local vehicle number conservation,

$$\frac{\partial}{\partial t}\rho(x,t) + \frac{\partial}{\partial x}[\rho(x,t)v(x,t)] = 0, \tag{2}$$

and an equation of motion,

$$\frac{\partial v}{\partial t} + v\frac{\partial v}{\partial x} = \mathcal{R}[V_{op}(\rho^{-1}) - v] - \mathcal{A}\frac{\partial \rho}{\partial x} + \mathcal{D}\frac{\partial^2 v}{\partial x^2}, \tag{3}$$

where $V_{op}(\rho^{-1})$ is the so-called optimal velocity function and the coefficients ($\mathcal{R}$ for the relaxation term, $\mathcal{A}$ for the anticipation term, and $\mathcal{D}$ for the diffusion term) are positive definite and depend in general on the density and velocity fields, i.e., $\mathcal{R}(\rho,v)$, $\mathcal{A}(\rho,v)$, and $\mathcal{D}(\rho,v) > 0$.

To find out steady-state solutions of the type in Eq. (1), it is useful to map the problem into a single-particle motion problem by using the method in Refs. [22,24]. For the mapping, one first integrates out Eq. (2). The resulting constant of motion

$$q_g = \rho(v + v_g) \tag{4}$$

relates two dynamic fields ρ and v, and can be used to reduce the number of independent dynamic fields from two to
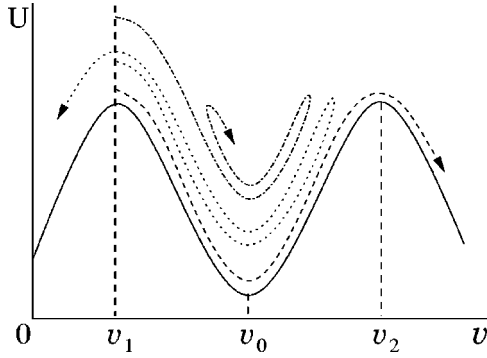
FIG. 1. A typical shape of the potential energy $U(v;v_g,q_g)$ (solid line). Three examples of the particle motion are also shown (dotted, dashed, and dash-dotted lines).
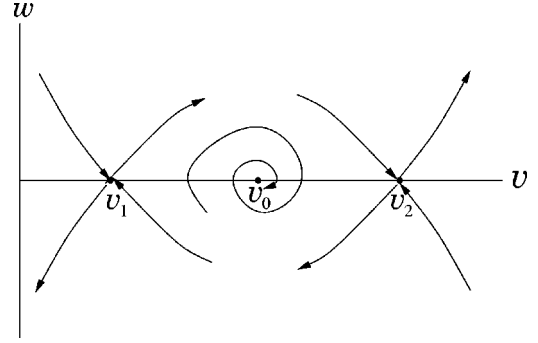

FIG. 2. A schematic diagram of the flow near the three fixed points $(v_{0,1,2},0)$. $\mathcal{C}$ is assumed to be positive near $v=v_0$ in this figure.

one (we choose v in this work). Then Eq. (3) can be transformed into an *ordinary* differential equation for the single dynamic field v that depends on a single parameter $z \equiv x + v_g t$,

$$\frac{d^2v}{dz^2} + \mathcal{C}(v;v_g,q_g)\frac{dv}{dz} + \mathcal{F}(v;v_g,q_g) = 0, \qquad (5)$$

where

$$\mathcal{C}(v;v_g,q_g) \equiv \frac{1}{\mathcal{D}}\left[\frac{\mathcal{A}q_g}{(v+v_g)^2} - (v+v_g)\right], \qquad (6)$$

$$\mathcal{F}(v;v_g,q_g) \equiv \frac{\mathcal{R}}{\mathcal{D}}(V_{op} - v).$$

Here the field ρ in the arguments of $\mathcal{R}$, $\mathcal{A}$, $\mathcal{D}$, and V_{op} should be understood as $q_g/(v+v_g)$. Then the search for steady-state solutions reduces to the analysis of Eq. (5) under the physically meaningful boundary condition that solutions should be bounded as $z \to \pm \infty$.

To gain insights into implications of Eq. (5), it is useful to make an analogy with a classical mechanics of a particle by regarding z as a time variable and v as a *coordinate* of a particle with unit mass moving in a one-dimensional system. Then Eq. (5) describes the time evolution of a particle under the influence of a potential energy $U(v;v_g,q_g) = \int^v dv' \mathcal{F}(v';v_g,q_g)$ and of a damping force with the coordinate-dependent damping coefficient $\mathcal{C}(v;v_g,q_g)$. For a physical choice of $V_{op}(\rho^{-1})$, which decreases as ρ increases, goes to zero for large ρ, and saturates at a finite value for small ρ, the potential energy U becomes *camelback shaped* for wide ranges of v_g and q_g (solid curve in Fig. 1). Thus the potential energy profile is of very typical shape. Below we focus on U of this shape only and ignore the possibility of more exotic shaped U's, such as U's with three peaks, since we do not know of any reason to expect such exotic possibilities. Furthermore, we will not address the trivial case occurring when the range of v_g and q_g allows less than two peaks in U.

An unusual feature in this mechanical analogy is that the damping coefficient $\mathcal{C}$ is *not* necessarily positive, and in

those ranges of v where $\mathcal{C}$ is negative, the particle may *gain* energy due to the damping. The possibility of the negative damping is crucial for the existence of certain steady-state solutions presented in the following section.

Before we close this section, we remark that the stability of a solution in the single-particle problem should not be identified with the stability in the real traffic problem. We demonstrate this point with trivial z-independent solutions. For the camelback-shaped potential in Fig. 1, extremal points of the potential become solutions. Thus there are three z-independent solutions, $v=v_i$ ($i=0,1,2$ and $0 \leq v_1 < v_0 < v_2$), where v_0 is the coordinate of the local minimum and v_1, v_2 are coordinates of the two local maxima or saddle points. All v_i's satisfy $V_{op}((v+v_g)/q_g)=v$ and thus depend on v_g and q_g. These z-independent solutions correspond to the homogeneous traffic states $v(x,t)=v_{0,1,2}$. From the shape of the potential energy, it is clear that in the single-particle problem, the two solutions $v(z)=v_{1,2}$ are unstable with respect to small deviations and the other solution $v(z) = v_0$ is stable (if $\mathcal{C}$ is positive near v_0). For the real traffic problem [described by Eqs. (2) and (3)], however, the solutions $v(x,t)=v_{1,2}$ are (usually) *stable* with respect to small deviations and $v(x,t)=v_0$ is linearly unstable.

III. FLOW DIAGRAMS

Besides the trivial static (z-independent) solutions, there also exist dynamic (z-dependent) solutions, some examples of which are shown in Fig. 1 (dotted, dashed, and dash-dotted lines). In the language of traffic flow, these dynamic solutions correspond to *steady* but *inhomogeneous* traffic flow states. For a systematic study of dynamic solutions, it is useful to introduce a two-dimensional phase space $(v,w \equiv dv/dz)$, where each trajectory in the phase space corresponds to a dynamic solution. Then finding all solutions for given v_g and q_g is equivalent to constructing a flow diagram in the phase space for the given v_g and q_g.

To gain an insight into flow diagram structures, it is useful to examine the flow near the three fixed points $(v=v_i,w=0)$'s. Figure 2 show flows near the three fixed points. The fixed points $(v_{1,2},0)$ are saddle points regardless of the sign of $\mathcal{C}$ near $v=v_{1,2}$ since the damping force alone [the second term in Eq. (5)] cannot reverse the direction of the particle

motion (that is, the sign of dv/dz) even if the damping coefficient is negative. On the other hand, the fixed point $(v_0,0)$ is a stable (unstable) fixed point of the flow diagram when the $\mathcal{C}$ is positive (negative) near $v=v_0$ ($\mathcal{C}$ is assumed to be positive in Fig. 2). Flows running out of or into the fixed points can be mutually interconnected and the way they are interconnected will in general depend on the values of v_g and q_g and affect the structure of the flow diagram.

To make our discussion concrete, we choose here a particular hydrodynamic model. We choose the coefficients in Eq. (3) as follows:

$$\mathcal{R}=\lambda, \quad \mathcal{A}=\frac{\lambda\eta}{2\rho^3}, \quad \mathcal{D}=\frac{\lambda}{6\rho^2}, \tag{7}$$

where $\eta\equiv dV_{\mathrm{op}}/d(\rho^{-1})$. As demonstrated in Ref. [26], this choice provides a macro-micro link between the hydrodynamic model [Eqs. (2) and (3)] and the microscopic optimal velocity model [3],

$$\ddot{y}_n=\lambda[V_{\mathrm{op}}(\Delta y_n)-\dot{y}_n], \tag{8}$$

where $y_n(t)$ represents the coordinate of the nth vehicle in a one-dimensional road and Δy_n is the distance to the preceding vehicle, $y_{n+1}-y_n$. But we remark that as far as steady-state solutions are concerned, the choice (7) is just one *particular* option, and most results presented below are not sensitively dependent on it. Results which are dependent on the choice will be stated so. For the parameters, values in Ref. [27] are used: $\lambda=2 \ \mathrm{sec}^{-1}$,

$$V_{\mathrm{op}}(y)=\frac{v_{\mathrm{mag}}}{2}\left[\tanh\frac{2(y-y_{\mathrm{ref}})}{y_{\mathrm{width}}}+c_{\mathrm{ref}}\right], \tag{9}$$

$v_{\mathrm{mag}}=33.6$ m/sec, $y_{\mathrm{ref}}=25.0$ m, $y_{\mathrm{width}}=23.3$ m, and $c_{\mathrm{ref}}=0.913$. For this c_{ref}, the maximum value of V_{op} is $[(1+0.913)/2]v_{\mathrm{mag}}$, which is slightly different from v_{mag}.

For this hydrodynamic model, the resulting flow diagram is shown for various values of v_g and q_g in Fig. 3. Note that depending on v_g and q_g, trajectories departing from the two saddle points $(v_{1,2},0)$ behave in different ways and thus the flow diagrams acquire *topologically* different structures. Since the structure of the flow diagram is closely linked to characters of nonhomogeneous steady-state solutions, it will be meaningful to divide the plane (v_g,q_g) according to the flow diagram structures, which is given in Fig. 4. The v_g-q_g plane is divided into six regions (regions I, II, . . . , VI). The flow diagram *within* each region is labeled accordingly in Fig. 3. On the boundary between two neighboring regions, (e.g., boundary $\mathbf{B}_{\mathrm{I,II}}$ between the region I and II) the flow diagram acquires structures topologically different from those within the regions, and on the special point (v_g^*,q_g^*), where all six boundaries join together, the flow diagram acquires a special structure still different from all others. Steady-state solutions contained in the flow diagrams are presented in the following section.
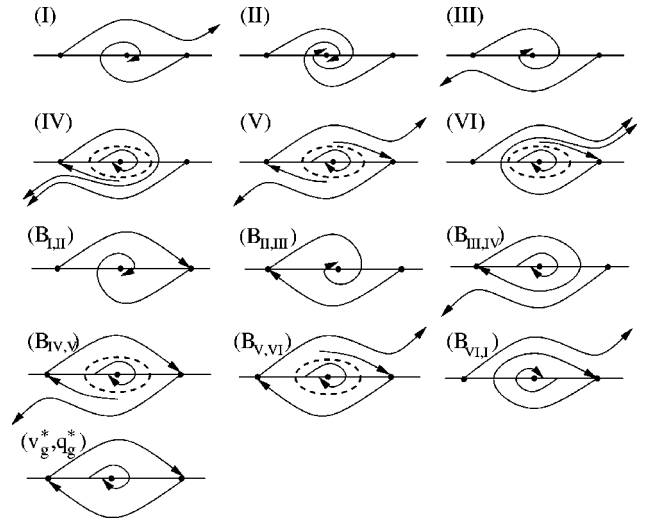

FIG. 3. Schematic drawings of the flow diagram in the phase space (v,w). Depending on the values of v_g and q_g, the flows running out of or into the fixed points are connected in different ways and as a result, the flow diagram acquires different topological structures. In each flow diagram, the fixed points $(v_{0,1,2},0)$ are marked by black circles. Emphasis is given to the flows running out of or into the fixed points in the range $v_1<v<v_2$.

IV. STEADY-STATE SOLUTIONS

Out of all flow trajectories contained in the flow diagrams (Fig. 3), only those trajectories that remain bounded both for $z\to\infty$ and $-\infty$ constitute physically meaningful steady-state solutions. Below we focus on those bounded trajectories.

A. Saddle-minimum solution

For each (v_g,q_q) in the regions I and II, there exists a single trajectory starting from the saddle point $(v_2,0)$ and converging to the potential minimum point $(v_0,0)$ [see Figs. 3(I,II)]. This trajectory represents the steady-state solution in Fig. 5(a). Similarly for each (v_g,q_g) in the regions II and III, there exists a single trajectory starting from the other saddle point $(v_1,0)$ and converging to the potential minimum point $(v_0,0)$ [see Figs. 3(II,III)]. The steady-state solution for this trajectory is similar to that in Fig. 5(a) except that the spatial profile approaches v_1 instead of v_2 as $z\to-\infty$. We call this type of steady-state solutions saddle-minimum solutions. We
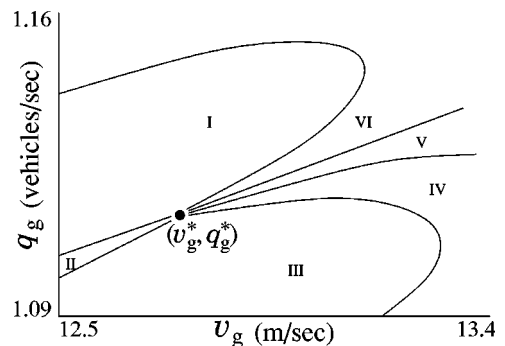

FIG. 4. The division of the parameter space (v_g,q_g) based on the topological structure of the flow diagram.
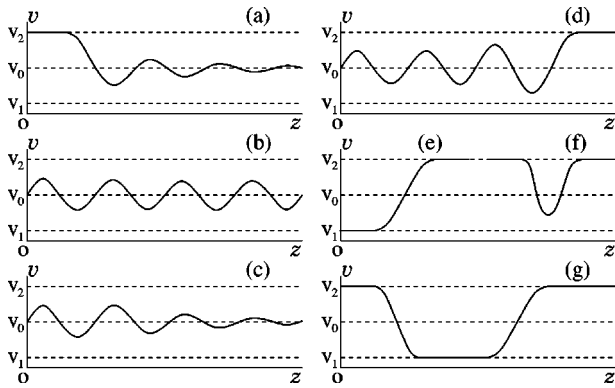
FIG. 5. Inhomogeneous steady-state solutions of a hydrodynamic model.

remark that the oscillation near v_0 may or may not appear depending on the parameter choice, which can be easily understood in the particle analogy; if the particle motion near v_0 is underdamped/overdamped, the convergence to v_0 in the saddle-minimum solution is oscillatory/nonoscillatory. Expansion of Eq. (5) near $(v_0,0)$ shows that the motion near v_0 is overdamped if $\lambda > 2$ and underdamped if $\lambda < 2$.

A study [25] on the optimal velocity model revealed that the microscopic model possesses so-called oscillatory traveling wave solutions and monotonic wave solution. These solutions are identical in their character to the saddle-minimum solution with the underdamped and overdamped convergence to v_0.

B. Limit-cycle solution

For each (v_g,q_g) in the region IV, V, or VI, there exists a single trajectory, which encircles the potential minimum point $(v_0,0)$ and makes a loop [see dashed curves in Figs. 3(IV,V,VI)]. In the language of nonlinear dynamics, this type of flow is usually referred to as a limit cycle. For traffic flow language, the limit cycle corresponds to a steady-state solution with periodic wave [Fig. 5(b)]. The "wavelength" of the limit-cycle solution increases and approaches infinity as (v_g,q_g) approaches (v_g^*,q_g^*). We remark that for the existence of the limit-cycle solution, it is crucial to have sign alternation of $\mathcal{C}$ with v. If $\mathcal{C}$ were always positive (negative), the single-particle motion analogy indicates that the total energy of the particle would monotonically decrease (increase) with z, and thus the trajectory would be attracted to (repelled away from) v_0, destroying the limit cycle.

Note that since there is a limit-cycle solution for each (v_g,q_g) within the regions IV, V, and VI, there is an infinite number of limit-cycle solutions, each with different (v_g,q_q). This feature is very similar to the report of many stable nonhomogeneous states in a revised car-following model in Ref. [18]. To our knowledge, it has not been realized previously that hydrodynamic models also possess infinitely many limit-cycle solutions.

C. Limit-cycle−Minimum solution

The limit-cycle solutions are inevitably accompanied by still different types of solutions. According to the flow diagrams in Figs. 3(IV,V,VI), all trajectories inside the limit cycle approach the minimum point $(v_0,0)$ as $z\to\infty$ and the limit cycle as $z\to-\infty$. We call this type of steady-state solutions limit-cycle−minimum solution. Its profile is shown in Fig. 5(c). Since there are infinitely many limit-cycle solutions and the limit-cycle−minimum solution is possible whenever the limit cycle is possible, there also exist infinitely many limit-cycle−minimum solutions.

This solution is closely related with an interesting phenomenon reported in previous studies of hydrodynamic models *with on-ramps* [14,15]: When a linearly unstable but convectively stable homogeneous flow is generated in the upstream part of an on-ramp, oscillatory flow is spontaneously generated from the homogeneous region and propagates in the upstream direction. The relation between this observation and the limit-cycle−minimum solution can be established by noting that the convectively stable homogeneous flow region corresponds to the trivial solution $v(z) = v_0$ and the spontaneously generated oscillatory flow to the limit-cycle solution. It is then clear that the phenomenon in Refs. [14,15] is nothing but a manifestation of the limit-cycle−minimum solution. Recent studies of a microscopic car-following model [16] also reported oscillatory flow growing out of a linearly unstable homogeneous region.

D. Limit-cycle−saddle solution

Each limit-cycle solution accompanies still another type of solutions. For each (v_g,q_g) in the regions IV and V, there exists a single trajectory converging to the saddle point $(v_1,0)$ as $z\to\infty$ and approaching the limit cycle as $z\to-\infty$ [Figs. 3(IV,V)]. Similarly for each (v_g,q_g) in the regions V and VI, there exists a single trajectory converging to the other saddle point $(v_2,0)$ as $z\to\infty$ and approaching the limit cycle as $z\to-\infty$ [Figs. 3(V,VI)]. We call this type of solutions limit-cycle−saddle solution. Its profile in the z space is shown in Fig. 5(d). Similar to the limit-cycle−minimum solutions, there exist infinitely many limit-cycle−saddle solutions.

E. Hetero-saddle-saddle solution

Still new types of bounded trajectories appear on the boundary $\mathbf{B}_{ij}$ between the region i and j. On the boundaries $\mathbf{B}_{I,II}$ and $\mathbf{B}_{IV,V}$, there is a trajectory running from the saddle point $(v_1,0)$ and converging to the other saddle point $(v_2,0)$ [Figs. 3 ($\mathbf{B}_{I,II}$), ($\mathbf{B}_{IV,V}$)]. This trajectory amounts to the kink solution in Fig. 5(e). Also on the boundaries $\mathbf{B}_{II,III}$ and $\mathbf{B}_{V,VI}$, there is a trajectory running from the *second* saddle point $(v_2,0)$ and converging to the *first* saddle point $(v_1,0)$ [Figs. 3 ($\mathbf{B}_{II,III}$), ($\mathbf{B}_{V,VI}$)]. Since the roles of $(v_1,0)$ and $(v_2,0)$ have been swapped, this trajectory amounts to the antikink solution [not shown in Fig. 5]. In the nonlinear dynamics language, these kinds of trajectories connecting two different fixed points are called heteroclinic orbits. In this paper, we will name this type of solutions hetero saddle-saddle solutions. To be more specific, we will call the first (second) type of the hetero-saddle-saddle solutions "upper" ("lower") hetero-saddle-saddle solutions since the trajectories appear in the upper (lower) half of the flow diagram. Note that there

exist infinitely many hetero-saddle-saddle solutions since this solution is allowed for each point (v_g, q_g) on the above-mentioned boundaries.

F. Homo-saddle-saddle solution

For each (v_g, q_g) on $\mathbf{B}_{VI,I}$, there exists a trajectory starting from the saddle point $(v_2, 0)$ and returning back to the *same* saddle point [Fig. 3 $(\mathbf{B}_{VI,I})$]. This trajectory represents the narrow cluster solution [Fig. 5(f)]. For each (v_g, q_g) on $\mathbf{B}_{III,IV}$, on the other hand, there exists a trajectory starting from the saddle point $(v_1, 0)$ and returning back to $(v_1, 0)$ [Fig. 3($\mathbf{B}_{III,IV}$)]. This trajectory represents the narrow anti-cluster solution (not shown in Fig. 5). In the nonlinear dynamics language, these kinds of trajectories are called homoclinic orbits. In this paper, we will name this type of solutions homo-saddle-saddle solutions. To be more specific, we will call the first (second) type of the homo-saddle-saddle solutions "right" ("left") homo-saddle-saddle solutions since the trajectories involve the saddle point on the right (left) half of the flow diagram.

G. Wide cluster solution

Figure 4 shows that all six regions and six boundaries meet together at a *single* point (v_g^*, q_g^*). The flow diagram at this point has a special structure [see Fig. 3(v_g^*, q_g^*)] that allows *smooth* connection between flow diagrams of different topological structure in different regions or boundaries.

This point is also special in the sense that the flow running out of the fixed point $(v_1, 0)$ reaches the other fixed point $(v_2, 0)$ and returns back to $(v_1, 0)$. The steady-state solution corresponding to this flow is shown in Fig. 5(g). Note that since the particle dynamics becomes infinitely slower as a trajectory approaches the fixed points $(v_{1,2}, 0)$, the cluster size of the steady-state solution is infinitely large. For this reason, we call this solution wide cluster solution.

The wide cluster solution is a limiting case of various solutions mentioned above; lf (v_g^*, q_g^*) is regarded as a limiting point of, for example, the boundary $\mathbf{B}_{III,IV}$ or $\mathbf{B}_{VI,I}$, the wide cluster solution is a homo-saddle-saddle solution with an infinite cluster size. If (v_g^*, q_g^*) is regarded as a limit point of the region VI, V, or VI, the wider cluster solution is a limit-cycle solution with an infinite period. Also if (v_g^*, q_g^*) is regarded as the point where the border lines $\mathbf{B}_{II,III}$ and $\mathbf{B}_{I,II}$ join, the wide cluster solution is a combined object of the upper hetero-saddle-saddle solution (kink) and the lower hetero-saddle-saddle solution (antikink).

The fact that the wide cluster solution is possible only at the single point (v_g^*, q_g^*) implies that the wide cluster solution has the so-called *universal* characteristics; when a given initial state of traffic evolves into the wide cluster solution following the real traffic dynamics [Eqs. (2) and (3)], characteristics such as outflow and the speed of the final traffic state are independent of the initial state.

Analyses [4,5] of empirical traffic data revealed that various characteristics of the wide jam are indeed universal. This empirical observation imposes a constraint on traffic models and the universality of the characteristics has been tested for traffic models. Although the universality has been verified for a number of traffic models [10,13,22,23], the verification unfortunately has relied largely on repeated numerical simulations and thus the verification itself is also "empirical" in some sense. One exceptional case is the analysis in Ref. [24], where the singular perturbation theory is used. This analysis is however considerably model dependent and thus it is not easy to perform the same analysis for other classes of traffic models. Contrarily, in our approach, the finding that the wide cluster solution can exist only at the single point (v_g^*, q_g^*) is quite meaningful since it explains clearly and unambiguously why the characteristics of the wide cluster solution should be universal.

We next address an interesting size dependence of the "wide cluster solution" reported in Ref. [22]; when numerical simulations are performed with periodic boundary conditions, the so-called universal characteristics are found [22,23] to be not strictly universal but depend on the system size. This size dependence is not compatible with the statement of the universality given above. To resolve this conflict, we first note that periodic boundary conditions allow only those solutions whose periods are compatible with the imposed period. Then the wide cluster solution, whose period is infinite, cannot be realized in such numerical simulations with finite system size, and the solutions, which are interpreted as the wide cluster solution in Refs. [22,23], are, strictly speaking, limit-cycle solutions whose periods are compatible with the imposed periodic boundary conditions. Then by recalling that there are infinitely many limit-cycle solutions, the size dependence is a very natural consequence and the conflict is resolved. We remark that the dependence however should become weaker as the period becomes longer since the limit-cycle solutions approach the wide cluster solution as their period becomes longer.

V. DISCUSSION

A. Roles of topology: Generality

As demonstrated in previous sections, each steady-state solution exists only in restricted regions of the v_g-q_g space where the flow diagram acquires certain topological structures. This relation between the steady-state solutions and the topological structure of the flow diagram is not a mere coincidence; all steady-state solutions presented in the preceding section are *guaranteed* to exist by the topologies of the flow diagrams. For example, when flows near the fixed point $(v_0, 0)$ is attracted towards $(v_0, 0)$ while flows running out of the other fixed points $(v_{1,2}, 0)$ are repelled away from $(v_0, 0)$, as in the regions IV,V,VI, there should exist the limit-cycle solution in those regions (Poincaré-Bendixson theorem [28]).

This relation with the topology bears an interesting implication. As demonstrated in many branches of physics, physical objects, whose existence is closely related with a certain topological structure of systems, are *not fragile* and their existence does *not* depend on quantitative details of the systems. Vortices in type-II superconductors are a well-known example. It is then expected that the steady-state solutions presented in the preceding section are not specific to the particular model examined but common to many versions of

hydrodynamic models. For example, our results are not sensitive to the values of the parameters in Eq. (9).

The generality due to the topology can be argued in the following way as well. Let us consider an infinitesimal change in the traffic model [in Eqs. (7) and (9) for example]. At (v_g, q_g) located sufficiently interior of a region in Fig. 4, the topological structure of the flow diagram will not be affected and thus all steady-state solutions, which are originally allowed in the region, are still allowed for the modified traffic model. On the other hand, at (v_g, q_g) located sufficiently close to a boundary in Fig. 4, the topological structure of the flow diagram may be modified to a new structure. However the only possible new structure is the one at just across the boundary. The net effect then amounts to a mere shift of the boundary. Thus as far as the topology is concerned, effects of the infinitesimal change in the traffic model are no more than shifting the boundaries of the six regions by infinitesimal amounts, and the existence of steady-state solutions in each region is *not* affected. Here we remark that despite the shifts, all six boundaries should still meet at a *single* point, whose coordinate may be slightly different from the original (v_g^*, q_g^*) though. Otherwise, continuous conversion of one topological structure to another near (v_g^*, q_g^*) is not possible.

Lastly we discuss briefly one special kind of modifications that shows negative-valued coefficient $\mathcal{C}$ [Eq. (6)] near the fixed point $(v_0, 0)$. In the hydrodynamic model proposed by Kerner *et al.* [2], $\mathcal{C}$ is indeed negative when the parameters in the model are set to the values suggested in Ref. [15]. For this case, the flow is *repelled* away from $(v_0, 0)$. Then the limit-cycle solution does not appear any more in the regions IV, V, VI but appears instead in the regions I, II, III. This shift is natural in view of the Poincaré-Bendixson theorem. However this negative $\mathcal{C}$ does not affect the very existence of the six regions because these are determined according to the trajectories departing from the two saddle points $(v_{1,2}, 0)$ as mentioned already. Thus our approach focused on the bounded trajectories between the four limiting behaviors (one limit cycle and three fixed points) is still valid. A more exotic kind of modifications are those, due to which $\mathcal{C}$ changes its sign multiple times with v so that multiple limit-cycle solutions exist for given v_g and q_g in certain regions of parameter space (v_g, q_g). However this possibility seems to be very unlikely since it requires considerable fluctuations of $\mathcal{A}$ [see Eq. (6)], which is unphysical.

B. Implications on universality conjecture

A conjecture has been put forward by Herrmann and Kerner [29]; many traffic models with different mathematical structures may belong to the same "universality" class in the sense that they predict same traffic phenomena. Although it is not clear yet to what extent the universality conjecture is valid, there are indications that there indeed exists close relationship between some traffic models. For example, macroscopic hydrodynamic models have been derived from a microscopic car-following model via certain approximation methods [26,30], and good agreement between two types of traffic models has been demonstrated via numerical simula-

tions [31]. In particular, an exact correspondence between two different types of microscopic models has been established [32]. We note in passing that the hydrodynamic model derived in Ref. [30] however has an instability that arises from short-wavelength fluctuations that are *not* present in the original car-following model. Such instability disappears when the short-wavelength fluctuations are properly regularized as in Ref. [26].

On the other hand, there exist reports which could not have been reconciled with the universality conjecture. For example, a recent study [18] on a certain special type of car-following model reported the existence of many limit-cycle solutions (even without intrinsic inhomogeneities on roads such as on-ramps). To our knowledge, the limit-cycle solution had not been reported for any other traffic models and thus it had been inferred that the limit-cycle solution might be specific to the special model, in clear contrast with the universality conjecture. Our results however indicate that this inference is wrong and reopen a possibility that the special car-following model may also be closely related to other traffic models. An evidence for this will follow in the following section.

By investigating topological structures of the flow diagrams, we found from a *single* traffic model *seven* inhomogeneous steady-state solutions. Although many of these solutions were already reported by earlier studies, earlier reports were scattered over various different traffic models and thus it was not clear whether a certain solution is specific to certain traffic models or generic to a wide class of models. Our analysis in the preceding section indicates that the seven inhomogeneous steady-state solutions are generic to a wide class of traffic models. Our results are thus valuable in view of the universality conjecture.

C. Prevalence of limit-cycle solution in Ref. [18]

As remarked above, most studies of traffic models failed to capture the limit-cycle solution. On the other hand, in the special car-following model studied in Ref. [18], a wide class of initial conditions evolve to the limit-cycle solution. A question arises naturally: what is special about the model in Ref. [18]? The model is defined as follows:

$$\ddot{y}_n = A\left(1 - \frac{\Delta y_n^0}{\Delta y_n}\right) - \frac{Z^2(-\Delta \dot{y}_n)}{2(\Delta y_n - \rho_m^{-1})} - kZ(\dot{y}_n - v_{\text{per}}),$$

(10)

where $Z(x) = (x + |x|)/2$, A is a sensitivity parameter, ρ_m^{-1} is the minimal distance between consecutive vehicles, v_{per} is the permitted velocity, k is a constant, and $\Delta y_n^0 \equiv \dot{y}_n T + \rho_m^{-1}$. Here T is the safety time gap. When interpreted in terms of the hydrodynamic model in Eq. (3), the first and third terms together define the effective optimal velocity $V_{\text{op}}^{\text{eff}}(\rho^{-1})$, which is shown in Fig. 6. The role of the second term is to strictly prevent the distance from being smaller than the minimum distance ρ_m^{-1} by establishing additional strong deceleration when a vehicle is faster than its preceding one and their separation approaches ρ_m^{-1}.
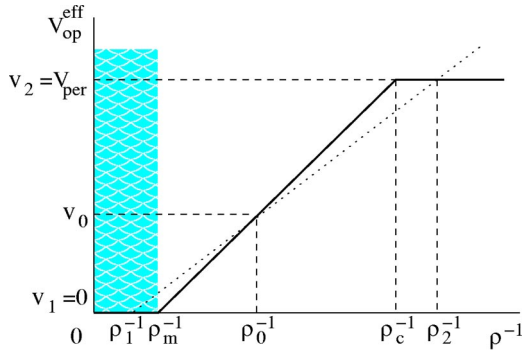
FIG. 6. The bold solid line is the effective optimal velocity V_{op}^{eff} due to the dynamics of Eq. (10). The dotted line on the other hand describes the constant of motion line in Eq. (4). The hatched region, where no dynamics is allowed, is established by the singular effect of the second term in Eq. (10). Three crossing points of the two lines determine the z-independent solutions of Eq. (5). Note that $\rho_c^{-1} = \rho_m^{-1} + Tv_{per}$.

In view of the steady-state analysis given in previous sections, the optimal velocity profile in Fig. 6 is very special: out of three solutions v_1, v_2, v_3 of $V_{op}^{eff}((v+v_g)/q_g) = v$, which amount to the extremal points of the potential U^{eff}, v_1 is *dynamically forbidden* since the vehicle spacing ρ_1^{-1} related to v_1 via Eq. (4) is shorter than ρ_m^{-1}, which is strongly prohibited by the second term in Eq. (10). Then steady-state solutions, such as wide cluster solution, that assume the accessibility to $(v_1, 0)$ are not allowed any more and the number of possible solutions reduces to 5 (saddle-minimum, limit-cycle, limit-cycle–minimum, limit-cycle–saddle, and homo-saddle-saddle solutions). Further reduction occurs when the periodic boundary condition is imposed as in Ref. [18]. Then homo-saddle-saddle and limit-cycle solutions are the only possible solutions. Among these two, the former is possible only when the average density satisfies $\rho < (\rho_m^{-1} + Tv_{per})^{-1}$ because the unique limiting behavior of that solution, of which density converges to ρ_2, will govern the average density and $\rho_2 < \rho_c$. Thus for the density range of $(\rho_m^{-1} + Tv_{per})^{-1} < \rho < \rho_m$, the limit-cycle solution is the only possible solution. Therefore the characteristics of the model in Ref. [18] are explained within the framework of the hydrodynamic approach.

D. Stability of solutions

The rigorous stability analysis, whether each solution above is realized through the dynamics in Eqs. (2) and (3),

goes beyond the scope of this work. In this section, we instead summarize what has been known and also discuss implications of existing results. The stability of the solution in Sec. IV G is well established [2,22]. For the solution in Sec. IV C, its relation with the oscillatory flow generated spontaneously out of a convectively stable homogeneous flow, which was reported in previous numerical simulations of hydrodynamic models with on-ramps [14,15], seems to indicate that this solution can be stable. Also the solution in Sec. IV B has been maintained stably in our own numerical simulation of the hydrodynamic model that is derived from the following microscopic model via the mapping rule in Ref. [26]:

$$\ddot{y}_n = \lambda[V_{op}^{eff}(\Delta y_n) - \dot{y}_n] + k\frac{\Delta \dot{y}_n}{\Delta y_n - \rho_m^{-1}}\Theta(-\Delta \dot{y}_n), \quad (11)$$

where V_{op}^{eff} is the same one depicted in Fig. 6, k is a constant, and $\Theta(x)$ is the Heavyside function (1 for $x > 0$ and 0 for $x < 0$). Note that the idea of the prevalence of the limit-cycle solution discussed in Sec. V C is simply reflected in Eq. (11). These observations suggest that at least some steady-state solutions addressed in this work can be maintained stably. However more systematic analysis is necessary to clarify the issue of the stability.

VI. CONCLUSION

Hydrodynamic traffic models are investigated by mapping them to the problem of single-particle motion. It is found that typical hydrodynamic models possess seven different types of inhomogeneous steady-state solutions. Although these solutions were already reported by earlier studies, earlier reports were scattered over various different traffic models and it was not clear whether a certain solution is specific to certain traffic models only or generic to a wide class of models. Our result combined with the topology argument indicates that the seven inhomogeneous steady-state solutions should be common to a wide class of traffic models. Also the origin of the universal characteristics for the wide cluster solution is clearly identified and the reason for the prevalence of the limit-cycle solution in a previous report [18] is provided.

ACKNOWLEDGMENT

---

[1] K. Nagel and M. Schreckenberg, J. Phys. I **2**, 2221 (1992); O. Biham, A.A. Middleton, and D. Levine, Phys. Rev. A **46**, R6124 (1992).

[2] B.S. Kerner and P. Konhäuser, Phys. Rev. E **48**, R2335 (1993).

[3] M. Bando, K. Hasebe, A. Nakayama, A. Shibata, and Y. Sugiyama, Phys. Rev. E **51**, 1035 (1995).

[4] I. Treiterer and J. A. Myers, in *Proceedings of the Sixth Inter-*

national Symposium on Transportation and Traffic Theory, edited by D. J. Buckley (Elsevier, New York, 1974); M. Koshi, M. Iwasaki, and I. Ohkura, in *Proceedings of the Eighth International Symposium on Transportation and Traffic Flow*, edited by V. F. Hurdle, E. Hauer, and G. N. Stewart (University of Toronto Press, Toronto, 1983).

[5] B.S. Kerner and H. Rehborn, Phys. Rev. E **53**, R4275 (1996);

Phys. Rev. Lett. **79**, 4030 (1997); B.S. Kerner, *ibid.* **81**, 3797 (1998); J. Phys. A **33**, L221 (2000); Phys. Rev. E **65**, 046138 (2002).

[6] L. Neubert, L. Santen, A. Schadschneider, and M. Schreckenberg, Phys. Rev. E **60**, 6480 (1999); W. Knospe, L. Santen, A. Schadschneider, and M. Schreckenberg, *ibid.* **65**, 056133 (2002).

[7] M. Treiber, A. Hennecke, and D. Helbing, Phys. Rev. E **62**, 1805 (2000).

[8] H.Y. Lee, H.-W. Lee, and D. Kim, Phys. Rev. E **62**, 4737 (2000).

[9] D. Chowdhury, L. Santen, and A. Schadschneider, Phys. Rep. **329**, 199 (2000); D. Helbing, Rev. Mod. Phys. **73**, 1067 (2001).

[10] T.S. Komatsu and S.I. Sasa, Phys. Rev. E **52**, 5574 (1995).

[11] T. Nagatani, J. Phys. Soc. Jpn. **66**, 1928 (1997).

[12] H.Y. Lee, H.-W. Lee, and D. Kim, Phys. Rev. Lett. **81**, 1130 (1998).

[13] D. Helbing and M. Treiber, Phys. Rev. Lett. **81**, 3042 (1998); D. Helbing and M. Schreckenberg, Phys. Rev. E **59**, R2505 (1999); V. Shvetsov and D. Helbing, *ibid.* **59**, 6328 (1999).

[14] D. Helbing, A. Hennecke, and M. Treiber, Phys. Rev. Lett. **82**, 4360 (1999).

[15] H.Y. Lee, H.-W. Lee, and D. Kim, Phys. Rev. E **59**, 5101 (1999).

[16] N. Mitarai and H. Nakanishi, J. Phys. Soc. Jpn. **68**, 2475 (1999); Phys. Rev. Lett. **85**, 1766 (2000); J. Phys. Soc. Jpn. **69**, 3752 (2000).

[17] W. Knospe, L. Santen, A. Schadschneider, and M. Schreckenberg, J. Phys. A **33**, L477 (2000); Phys. Rev. E **65**, 015101

(2002); J. Phys. A **35**, 3369 (2002).

[18] E. Tomer, L. Safonov, and S. Havlin, Phys. Rev. Lett. **84**, 382 (2000).

[19] P. Nelson, Phys. Rev. E **61**, R6052 (2000).

[20] I.A. Lubashevsky and R. Mahnke, Phys. Rev. E **62**, 6082 (2000); I. Lubashevsky, S. Kalenkov, and R. Mahnke, *ibid.* **65**, 036140 (2002); R. Kühne, R. Mahnke, I. Lubashevsky, and J. Kaupužs, *ibid.* **65**, 066125 (2002); I. Lubashevsky, R. Mahnke, P. Wagner, and S. Kalenkov, *ibid.* **66**, 016117 (2002).

[21] L.A. Safonov, E. Tomer, V.V. Strygin, Y. Ashkenazy, and S. Havlin, Europhys. Lett. **57**, 151 (2002); E. Tomer, L. Safonov, N. Madar, and S. Havlin, Phys. Rev. E **65**, 065101 (2002).

[22] B.S. Kerner and P. Konhäuser, Phys. Rev. E **50**, 54 (1994).

[23] S. Wada and H. Hayakawa, J. Phys. Soc. Jpn. **67**, 763 (1998).

[24] B.S. Kerner, S.L. Klenov, and P. Konhäuser, Phys. Rev. E **56**, 4200 (1997).

[25] P. Berg and A. Woods, Phys. Rev. E **63**, 036107 (2001).

[26] H.K. Lee, H.-W. Lee, and D. Kim, Phys. Rev. E **64**, 056126 (2001).

[27] S.-I. Takaki, M. Kikuchi, Y. Sugiyama, and S. Yukawa, J. Phys. Soc. Jpn. **67**, 2270 (1998).

[28] E.A. Jackson, *Perspectives of Nonlinear Dynamics* (Cambridge University Press, Cambridge, England, 1989), Vol. 1.

[29] M. Herrmann and B.S. Kerner, Physica A **255**, 163 (1998).

[30] P. Berg, A. Mason, and A. Woods, Phys. Rev. E **61**, 1056 (2000).

[31] D. Helbing, A. Hennecke, V. Shvetsov, and M. Treiber, Math. Comput. Modell. **35**, 517 (2002).

[32] J. Matsukidaira and K. Nishinari, Phys. Rev. Lett. **90**, 088701 (2003).